Journal of Geomatics Vol. 18, No. 1, April 2024

Aberrant variations in land, oceanic, and atmospheric parameters precedent to earthquakes

Kunvar S Yadav, Jahvi M. Patel*, Hani P. Patel, Govindchandra K. Patel, Rakesh B. Vadnatahani
Department of Physics, Mehsana Urban Institute of Sciences, Ganpat University, Mehsana-384012, Gujarat, India
*E-mail: kunvar.yadav@gmail.com

(Received on 30 July 2023; Accepted on 03 Apr 2024)

DOI: *https://doi.org/10.58825/jog.2024.18.1.100*

Abstract: Our Investigation provides valuable insights into the intricate interplay of environmental parameters leading up to significant earthquakes. By examining the SLHF, SST, CLW, and water-vapour, our study unveils distinctive behaviour in the data during the period spanning June 2021 to June 2022, coinciding with seismic events. The seasonal plots offer a visual representation of the variations in SLHF, SST, CLW, and water-vapour across different locations. These geographical depictions serve as a powerful tool for understanding the nuanced responses of these parameters before seismic activities. The overarching goal of our research is to shed light on the dynamic nature of these environmental factors, particularly when earthquakes occur near or beneath oceanic regions. This exploration not only contributes to the field of seismology but also has broader implications for comprehending the interconnected dynamics of land, ocean, and atmosphere in response to seismic phenomena. As we unravel the intricate relationship between these parameters and earthquake occurrences, our findings may pave the way for enhanced earthquake prediction and mitigation strategies.

Keywords: surface latent heat flux (SLHF), sea surface temperature (SST), cloud liquid water (CLW), water vapour (WV), earthquake

1. Introduction

Researchers are showing increased interest in detecting anomalies in land, ocean, and atmospheric parameters to improve the probability of earthquake prediction (Liu et.al 2001; Pulinets & Boyarchuk, 2004; Singh et.al, 2010). Complementary nature of surface and atmospheric parameters associated with Haiti earthquake of 12 January 2010 (Tronin A. A., 2000; Xu T., et al., 2011; Yadav et.al, 2016; Zhang et.al., 2022). These earthquakes have caused deaths, property loss, and impacted planning. Satellite remote sensing techniques have been used to examine the earthquake predictors over the earthquake ground zone at various heights before the seismic events. This study examined various land, oceanic, and atmospheric parameter changes, including SST, SLHF, CLW, and Water Vapour. The current research presents the results of multi-sensor data collected from various sources such as Microwave Climate Data Centre (MCDC), IRI/LDEO Climate Data Library's national centre for environmental prediction analysis project (NOAA). These statistics cover the period associated with the eleven earthquakes indicated in Table 1 that occurred in various regions of the globe. The heat released by phase changes caused by solidification, evaporation, or melting is represented by surface latent heat flux (SLHF), a significant component of the Earth's energy budget. The SLHF strongly depends on climatological variables such as wind speed, relative humidity, ocean depth, and sea surface temperature (SST) (Dey & Singh, 2003; Ghosh, et. al., 2020; Ghosh, et al., 2022; Jie & Guangmeng, 2014; Kumar et. al., 2021; Schulz, et.al., 1997; Singh et.al., 2002; Xu T, et al., 2011; (Yadav et.al., 2016). They suggested SLHF as a predictor of seismic activity in the coastal zone; they discovered some abnormal SLHF peaks a few days ahead of 5 earthquakes close to the coast (Dey & Singh, 2003). Changes in sea surface temperature (SST) are believed to be a precursor to earthquakes and also influence variations in surface latent heat flux (SLHF) (Dey & Singh, 2003; Ghosh, et al., 2020; Ghosh, et. al., 2022; Tronin A. A., 2000; Xu T., et al., 2011; Yadav et.al., 2016). The temperature of the water, which is referred to as SST, is affected by the air masses present in the atmosphere close to the surface of the ocean. Anomalies in SST and SLHF were observed during the Bourmerdes earthquake that occurred in May 2003, which had a magnitude of 6.8 (Ouzounov et. al., 2006) and Sumatra earthquake in December 2004 (Singh, et. al., 2007) and China January 10, 1998, and Kobe, Japan, on January 17, 1995 (Tronin et. al., 2002) and Loyalty Island earthquake in January 2009 (M = 6.6) (Yadav et.al., 2016) and Gangtok, India earthquake on September 18, 2011 (M = 6.9) (Kumar et..al., 2021)] and Kathmandu, Nepal earthquake on April 25 & May 12, 2015 (Ghosh, et. al., 2022) as well as Maduo Country, Qinghai earthquake on May 21, 2021 (M = 7.4) and Nima Country, Tibet earthquake on July 22, 2020 (M = 6.6) (Xu et.al., 2021). Earlier researchers motivated us to examine the parameters SLHF, SST, CLW, and Water Vapour - to determine whether anomalies behaviour in the land, ocean, and atmosphere are related (Dey & Singh, 2003; Singh, et al., 2002; Singh, et al., 2007). It has been noted that earthquakes cause changes in the characteristics of the land, ocean, and atmospheric parameters. These studies imply that the earthquake may have been related to the land, ocean, and atmosphere. Water vapour is one of the leading Greenhouse Gases (GHGs) in the atmosphere and the main gaseous absorber of infrared radiation in the atmosphere. Therefore, it is essential to understand how the global rise in other GHGs, particularly carbon dioxide, would change the amount of water vapor and its distribution in the atmosphere (Bobylev et.al., 2009; Jing et.al., 2013; Singh, et al., 2007; Singh et.al., 2010). According to current predictions, the amount of water vapour in the atmosphere should rise as the energy is released from the Earth's surface. Thus, an increase in saturation water vapour pressure and, ultimately, an

increase in water vapour concentration should result from the atmosphere warming induced by rising carbon dioxide levels. Multiple researchers are currently being conducted to calculate water budget and recycling ratios (the percentage of precipitation over a region that originated as evaporation from that same region), indicators of water vapour amount in the atmosphere (Bobylev et.al., 2009). Cloud liquid water impacts the radiation that reaches the Earth's surface and significantly affects the energy flux at the surface, which in turn influences the climate system (Bobylev et.al., 2009; Greenwald et.al., 1993; Jing et..al., 2013; Ouzounov & Freund, 2001; Singh, et al., 2007; Singh, et.al., 2010; Xu et.al., 2021). Hence, it is essential to conduct long-term, high-quality, regularly updated measurements of atmospheric water vapour and cloud liquid water content, particularly measurements in the vicinity of the seismic zone. Many researchers hypothesized that the ionospheric disturbance was brought about by the Earth's surface emitting radon gas before the earthquake, which then ionized the air near the ground, causing water vapour to condense and latent heat to be released (Bowen, 2012; Chavalier, 2007; Pulinets et. al., 2018). They are necessary for separating climate variability from cyclical fluctuations in the climate and studying the variability and trends of these parameters. We studied multi-sensor characteristics like SST, SLHF, CLW, and Water Vapor derived from satellite data, which are openly accessible and high-quality data. The paper analyzes land, ocean, and atmosphere parameters before and after earthquakes to observe their possible connection.

The figure 1shows the location of earthquakes listed in table 1.

Table 1. Details of earthquakes

Sr. No.	Location & magnitude of the epicentre	(Latitude, Longitude) of epicentre	Date	Time (UT)
1	Vallenar, Chile & (M = 6.0)	(28º44′ S, 71º28′ W)	July 4, 2021	01:29
2	Burica, Panama & (M = 6.7)	(7º23′ N, 82º46′ W)	July 21, 2021	21:15
3	Hukay, Philippines & (M = 6.7)	(13º42′ N, 120º43′E)	July 23, 2021	20:48
4	Sk, Russia & (M = 6.0)	(48º51′ N, 154º54′ E)	August 24, 2021	05:37
5	Yilan, Taiwan & (M = 6.2)	(24º30′ N, 121º49′ E)	October 24, 2021	05:11
6	Masachapa, Nicaragua & (M = 6.3)	(11º13′ N, 86º31′ W)	November 9, 2021	06:25
7	Concepcian, Guatemala & (M = 6.2)	(14º08′ N, 91º23′ W)	February 16, 2022	07:12
8	Cabra, Philippines & (M = 6.4)	(14º05′ N, 119º22′ E)	March 13, 2022	21:05
9	Namie, Japan & (M = 7.3)	(37º42′ N, 141º34′ E)	March 16, 2022	14:36
10	Hualien City, Taiwan & (M = 6.7)	(23º23′ N, 121º36′ E)	March 22, 2022	17:41
11	Namuac, Philippines & (M = 6.0)	(19º01′ N, 121º21′ E)	June 30, 2022	18:40

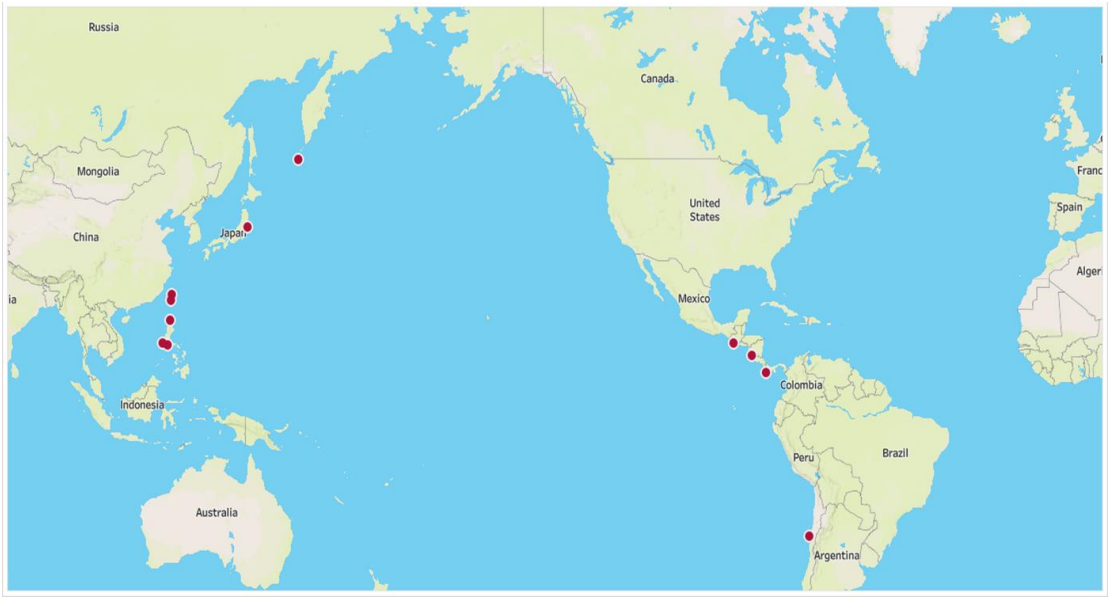

Figure 1. The map shows the location of earthquakes. Where, brown-coloured dots show earthquake locations.

2. Data and Analysis

2.1. Earthquake data

Many disastrous earthquakes have happened recently at or beneath the seafloor, sometimes close to an ocean. In this study, we explore the earthquakes that occurred in Vallenar, Chile; Burica, Panama; Hukay, Philippines; Sk, Russia; Yilan, Taiwan; Masachapa, Nicaragua; Hualien City, Taiwan; Concepcian, Guatemala; Cabra, Philippines; Namie, Japan and Namuac, Philippines. The primary selection criteria are a magnitude of at least 6.0 and proximity to an ocean's surface. The epicentral positions for the chosen earthquakes are provided in Table 1. It collected a list of the earthquakes that happened in June 2021 to June 2022. The following link to download the earthquake list:(https://earthquake.usgs.gov/earthquakes/search/)

2.2 Remote sensing data

Microwave Climate Data Centre (MCDC) (https://data.remss.com/amsr2/ocean/L3/v08.2/daily/) provided the multi-sensor parameter SST, CLW, and Water Vapor data. The SLHF data were obtained from the IRI/LDEO climate data library's National Centre for Environmental Prediction Analysis Project (NOAA) (https://iridl.ldeo.columbia.edu/SOURCES/.NOAA/.NCEP-NCAR/). The averaged values are multi-year mean is subtracted from daily variation to find the anomalies. Represented as:

$$anomaly = \left[\frac{value - mean}{std.deviation}\right] \times 100\%$$

The mean values have been used over the past seven years of data. The SST, CLW, and Water Vapor data were received in NetCDF format and translated to CSV format using Python. The SLHF data were received in a raw file. Then PHP program was used to analyze these data. The presented results in this article show changes in SLHF, SST, CLW, and Water Vapor to exhibit changes in land, ocean, and atmospheric parameters before and after the earthquake.

3. Result And Discussion

Multi-sensor parameters for the prediction of earthquakes have been presented by many researchers. (Bobylev et.al., 2009) developed a new algorithm utilizing neural networks to retrieve atmospheric water vapor and cloud liquid water content from satellite microwave radiometer data in high-latitude open-water areas. (Dey & Singh, 2003) showed uncommon variations in SLHF 2-7 days before the major earthquake event resulting from ocean-land-atmospheric interactions. Which was linked to the increased infrared thermal (IR) temperature. (Jing et.al., 2013) showed that anomalies in outgoing longwave radiation, surface latent heat flux, air temperature, relative humidity, and air temperature might be the cause of a major earthquake in Wenchuan on May 12, 2008. In their study, outgoing longwave radiation seemed to be the first parameter to be observed as an early warning signal. While air temperature, relative humidity, and air pressure demonstrated quasi-simultaneous variations in both the basin and the mountain region near the epicentre. SLHF exhibited its anomaly one day prior to the seismic event. (Kumar et.al., 2021) did 42 years of study of SLHF in the Indian subcontinent to see the precursor effects of earthquakes on it. A notable average increase in SLHF was 10-15 before the earthquakes were recorded. Their study also showed background noise levels in the epicentre regions of ten earthquakes over the past 42 years. Singh, et al., 2007 showed a strong coupling between the ocean, land, meteorological and atmospheric parameters before and after the Sumatra main event of 26 December 2004(Singh et.al., 2010) showed changes in the humidity from the surface up to altitude 500 hPa, which clearly showed the atmospheric perturbations associated with the earthquake event.

Their paper also showed that ozone concentration was found to be lowest on the earthquake day and found to be increased within a week of the earthquake.; (Yadav et.al., 2016) showed SST variations prior to three earthquakes in coastal regions causing SLHF to change. An ionosphere parameter called TEC (Total Electron Content) has been displayed here, which shows anomalous variations 1-13 days prior to the earthquake. We have plotted here the long-term data of each location for the period of one year, and the plot of every season shown in the present paper (Figure 2(a-d) to 12(a-d)). - This study focuses on using multi-sensor parameters from land, ocean, and atmosphere anomalies to detect earthquake precursors. Table 2 overviews the SLHF, SST, CLW, and Water Vapour improvement before all earthquakes.

3.1 Multi-Sensor Parameters

To identify anomalies in SST, SLHF, CLW, and Water Vapor analysed, epicentres close to the ocean have been chosen. The SLHF depends on the seasons because it is a function of surface temperature. Additionally, it is influenced by the region's characteristics and how close it is to the sea. The term "latent heat" (SLHF) refers to the amount of heat absorbed or released during a phase transition, such as melting, evaporation, or solidification. Before an earthquake, the coastal region experiences stress build-up that causes thermal infrared emission, speeding up the rate of energy transfer between the surface and atmosphere and raising SLHF (Dey & Singh, 2003; Ghosh, et al., 2022; Jie & Guangmeng, 2014). These links imply that interactions between the near-Earth environment and the land will continue (Ouzounov & Freund, 2004; Singh, et al., 2001]. Surface temperature variation, which is meant to be a parameter that indicates an earthquake, controls the fluctuation in SLHF (Ouzounov & Freund, 2004; Singh, et al., 2001; Tronin, 1999). Anomaly in positive peaks have been observed in SST, SLHF, CLW, and Water Vapour anomalies in different seasons (Figure 2(a-d) to 12(a-d)).

Table 2. Summarizes the information and findings for all 11 earthquakes mentioned in the study

Sr. no.	Location of the epicentre (Latitude, Longitude) & Magnitude	Date	SST anomalies prior to EQ	SLHF anomalies prior to EQ	CLW anomalies prior to EQ	WV anomalies prior to EQ
1	Vallenar, Chile (28º44′ S, 71º28′ W) & (M = 6.0)	July 4, 2021	13, 30 days (Figure 2(c))	5, 23 days (Figure 2(c))	5, 19 days (Figure 2(c))	1, 15 days (Figure 2(c))
2	Burica, Panama (7º23′ N, 82º46′ W) & (M = 6.7)	July 21, 2021	16, 21 days (Figure 3(c))	12, 24 days (Figure 3(c))	1, 11, 26, 30 days (Figure 3(c))	7, 22 days (Figure 3(c))
3	Hukay, Philippines (13º42′ N, 120º43′ E) & (M = 6.7)	July 23, 2021	23 days (Figure 4(c))	1, 17 days (Figure 4(c))	14, 40 days (Figure 4(c))	1, 4, 8 days (Figure 4(c))
4	Sk, Russia (48º51′ N, 154º54′ E) & (M = 6.0)	Aug 24, 2021	3, 30 days (Figure 5(c))	8, 12 days (Figure 5(c))	9, 11, 16, 26 days (Figure 5(c))	1, 13, 27 Days (Figure 5(c))
5	Yilan, Taiwan (24º30′ N, 121º49′ E) & (M = 6.2)	October 24, 2021	4, 11, 14, 20 days (Figure 6(d))	2, seven days (Figure 6(d))	28, 30 days (Figure 6(d))	3, 24, 28 days (Figure 6(d))
6	Masachapa, Nicaragua (11º13′ N, 86º31′ W) & (M = 6.3)	November 9, 2021	5, 15 days (Figure 7(d))	6, 12 days (Figure 7(d))	22, 27 days (Figure 7(d))	4, 22, 28 days (Figure 7(d))
7	Concepcian, Guatemala (14º08′ N, 91º23′ W) & (M = 6.2)	February 16, 2022	12, 18, 23 days (Figure 8(a))	2, 10, 16 days (Figure 8(a))	10, 17, 20 days (Figure 8(a))	2, 6, 20, 33 days (Figure 8(a))
8	Cabra, Philippines (14º05′ N, 119º22′ E) & (M = 6.4)	March 13, 2022	2, 12 days (Figure 9(b))	4, 12 days (Figure 9(b))	3, 10 days (Figure 9(b))	7, 11, 13, 15 days (Figure 9(a, b))
9	Namie, Japan (37º42′ N, 141º34′ E) & (M = 7.3)	March 16, 2022	3, 10 days (Figure 10(b))	10, 14 days (Figure 10(b))	2, 6, 10 days (Figure 10(b))	2, 5, 12 days (Figure 10(b))
10	Hualien City, Taiwan (23º23′ N, 121º36′ E) & (M = 6.7)	March 22, 2022	1, 16 days (Figure 11(b))	5,16 days (Figure 11(b))	4, 8 days (Figure 11(b))	19 days (Figure 11(b))
11	Namuac, Philippines (19º01′ N, 121º21′ E) & (M = 6.0)	June 30, 2022	8 days (Figure 12(c))	2, 8 days (Figure 12(c))	2, 6, 20, 29 days (Figure 12(c))	6, 16 days (Figure 12(c))

From figure 2(c), it can be seen that the high value of SLHF from June 24 to June 30, 2021, is what caused the abnormal increase in SST from 17 to June 21, 2021, and the increment of Water Vapour from June 29 to July 3, 2021, and also abnormal increase in CLW from June 28 to July 1, 2021, that preceded the earthquake that occurred on July 4, 2021, in the Vallenar, Chile region in Winter. As seen in figure 3(c), SST increased between July 2 to July 6, 2021, and immediately following this improvement in SST, SLHF increased abnormally between 04 to July 11, 2021, CLW increased from 07 to July 12, 2021, and also increase Water Vapour from 11 to July 16, 2021, soon before the Burica, Panama earthquake in Summer on July 21, 2021.

From Figure 4(c), it can be seen that the high value of SLHF from July 2 to July 6, 2021, is what caused the abnormal increase in SST from June 28 to July 2, 2021, and the increment of Water Vapour from July 12 to July 19, 2021, and also abnormal increase in CLW from July 7 to July 11, 2021, that preceded the earthquake that occurred on July 23, 2021, in the Hukay, Philippines region in Summer. The most significant anomalies (> 500% Normalised Anomaly) in SLHF are shown from 09 to August 14, 2021 (Figure 5(c)) before the earthquake at Severo-Kuril Sk, Russia, in Summer on August 24, 2021, as a result of an increase in SST from July 24, 2021, to July 26, 2021 (Figure 5(c)), Water Vapor is shown from 08 to August 11, 2021 (Figure 5(c)) and also increase in CLW from 06 to August 10, 2021 (Figure 5(c)).

From figure 6(d), it can be seen that the high value of SLHF from October 13 to October 19, 2021, is what caused the abnormal increase in SST from October 8 to October 14, 2021, and the increment of Water Vapour from October 19 to October 22, 2021, and also abnormal increase in CLW from September 21 to September 24, 2021, that preceded the earthquake that occurred on October 24, 2021, in the Yilan, Taiwan region in Autumn.

As seen in figure 7(d), SST increased between October 31 to November 5, 2021, and immediately following this improvement in SST, SLHF increased abnormally between October 30 to November 4, 2021, CLW increased from 18 to October 21, 2021, and also increased Water Vapour from October 31 to November 4, 2021, soon before the Masachapa, Nicaragua earthquake in Autumn on November 9, 2021. From figure 8(a), it can be seen that the high value of SLHF from January 29 to February 14, 2022, is what caused the abnormal increase in SST from January 22 to January 26, 2022, and the increment of Water Vapour from 07 to February 13, 2022, and also abnormal increase in CLW from February 5 to February 10, 2022, that preceded the earthquake that occurred on February 16, 2022, in the Concepcion, Guatemala region in Winter. As seen in figure 9(a), SST increased between 23 to February 26, 2022, and immediately following this improvement in SST, SLHF increased abnormally between 04 to March 11, 2022, in figure 9(b), CLW increased from 06 to March 12, 2022, in figure 9(b) and also increase Water Vapour from February 25, 2022 (Figure 9(a)) to March 1, 2022, soon before the Cabra, Philippines earthquake in Spring on March 13, 2022.

The significant anomalies in SLHF are shown from 04 to March 8, 2022 (Figure 10(b)) before the earthquake at Namie, Japan, in Spring on March 16, 2022, as a result of an increase in SST from March 4, 2022, to March 9, 2022 (Figure 10(b)), Water Vapour is shown from 08 to March 13, 2022 (Figure 10(b)) and also (> 300% Normalised Anomaly) increase in CLW from 08 to March 13 (Figure 10(b)). From figure 11(b), it can be seen that the high value of SLHF from March 3 to March 12, 2022, is what caused the abnormal increase in SST from March 4 to March 7, 2022, and the increment of Water Vapour from March 13 to March 15, 2022, and also abnormal increase in CLW from March 12 to March 16, 2022, that preceded the earthquake that occurred on March 22, 2022, in the Hualien City, Taiwan region in Spring.

The significant anomalies in SLHF are shown from 24 to June 28, 2022 (Figure 12(c)) before the earthquake at Namuac, Philippines, in Summer on June 30, 2022, as a result of an increase in SST from June 22, 2022, to June 25, 2022 (Figure 12(c)), Water Vapour is shown from 21 to June 25, 2022 (Figure 12(c)) and also increase in CLW from 21 to June 25, 2022, and 27 to June 29, 2022 (Figure 12(c))

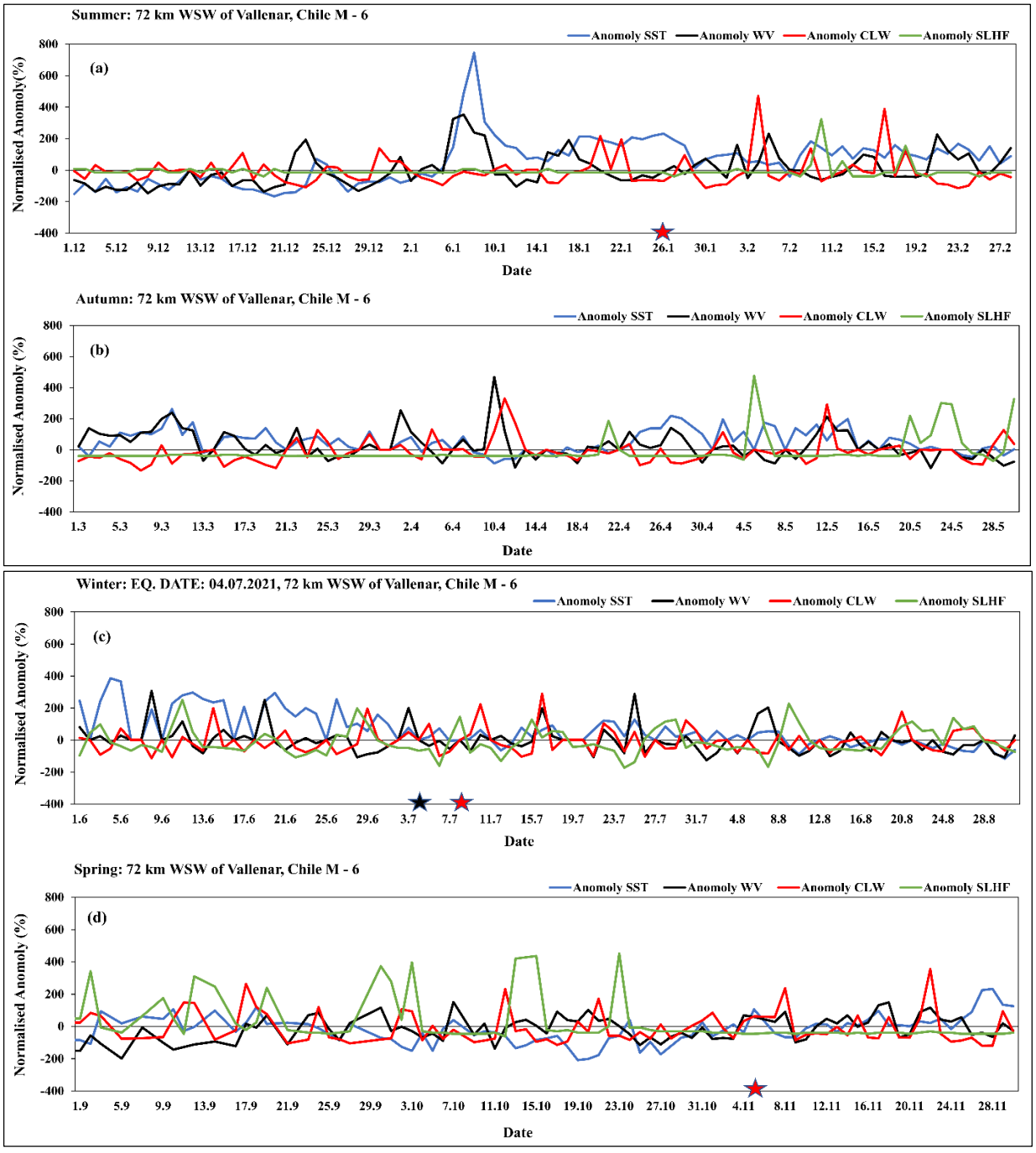

Figure 2. (a), (b), (c), (d) shows the graph of summer, autumn, winter and spring respectively. The black star indicates day of earthquake with M ≥ 6. The red star indicates the day of the earthquake with 4.5 ≤ M < 6. Before the earthquake, SST is followed by SLHF and observed the increments of CLW and Water Vapour.

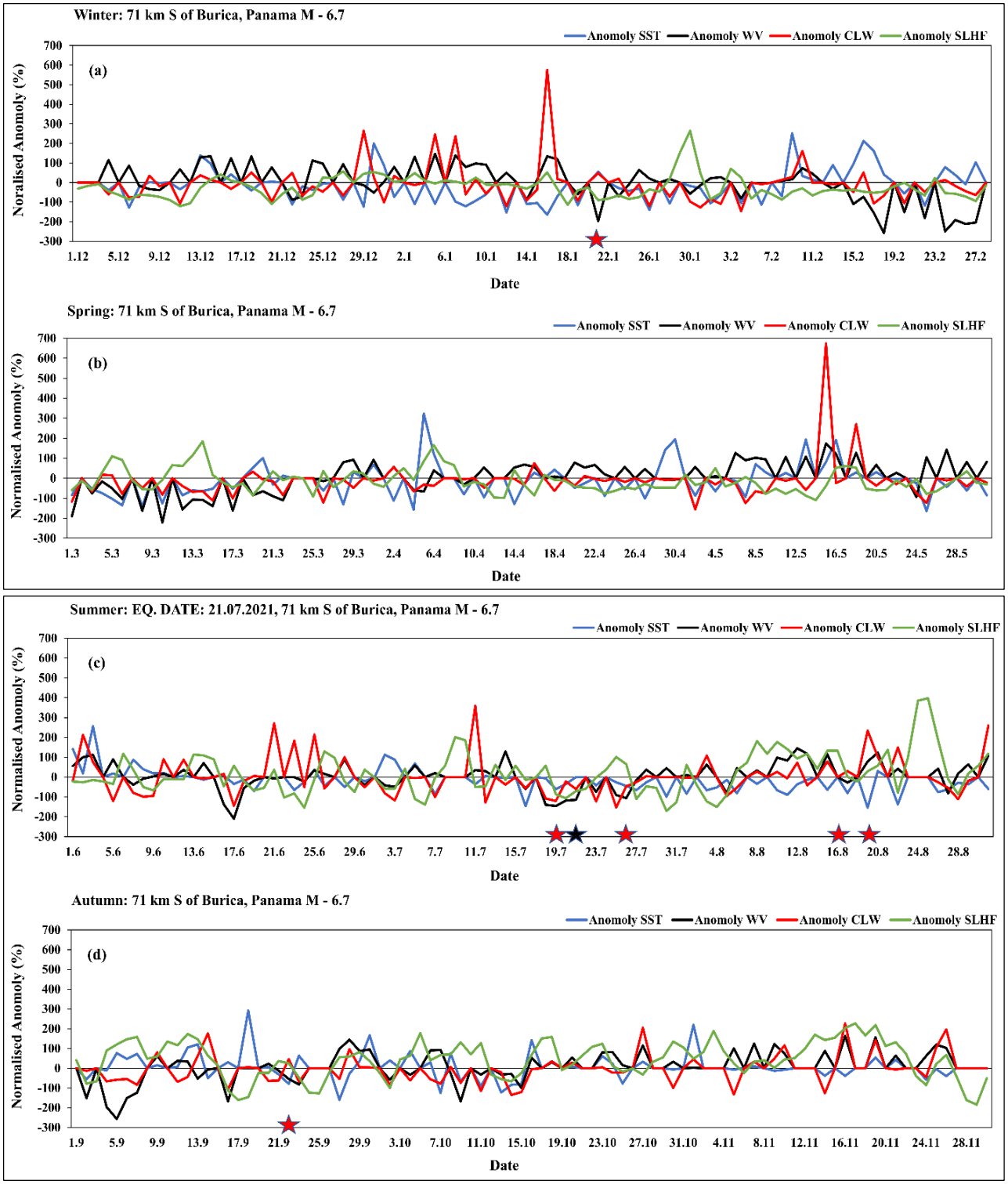

Figure 3. (a), (b), (c), (d) shows the graph of winter, spring, summer and autumn respectively. The black star indicates day of earthquake with M ≥ 6. The red star indicates the day of the earthquake with 4.5 ≤ M < 6. Before the earthquake, SST is followed by SLHF and observed the increments of CLW and Water Vapour.

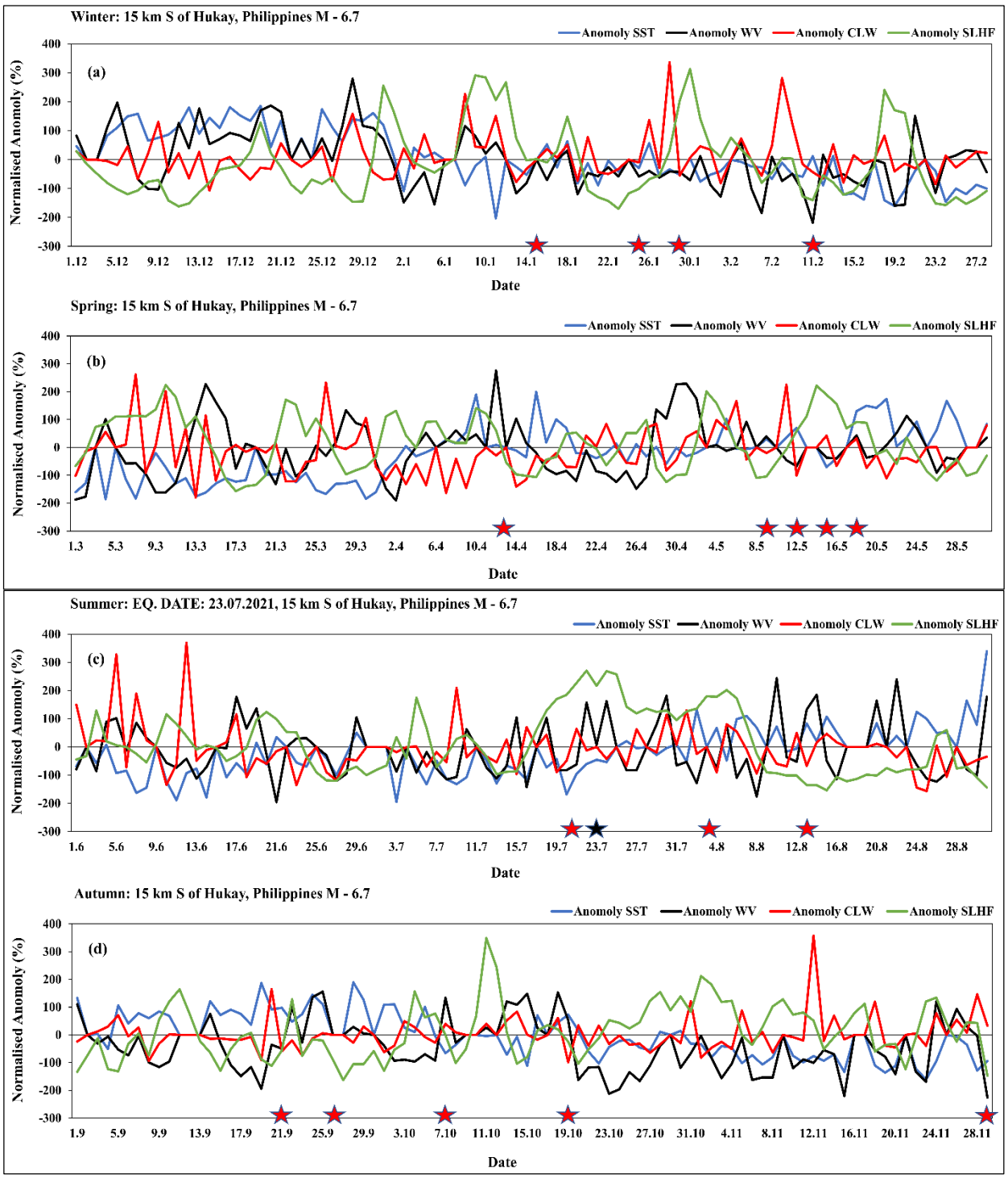

Figure 4. (a), (b), (c), (d) shows the graph of winter, spring, summer and autumn respectively. The black star indicates day of earthquake with M ≥ 6. The red star indicates the day of the earthquake with 4.5 ≤ M < 6. Before the earthquake, SST is followed by SLHF and observed the increments of CLW and Water Vapour.

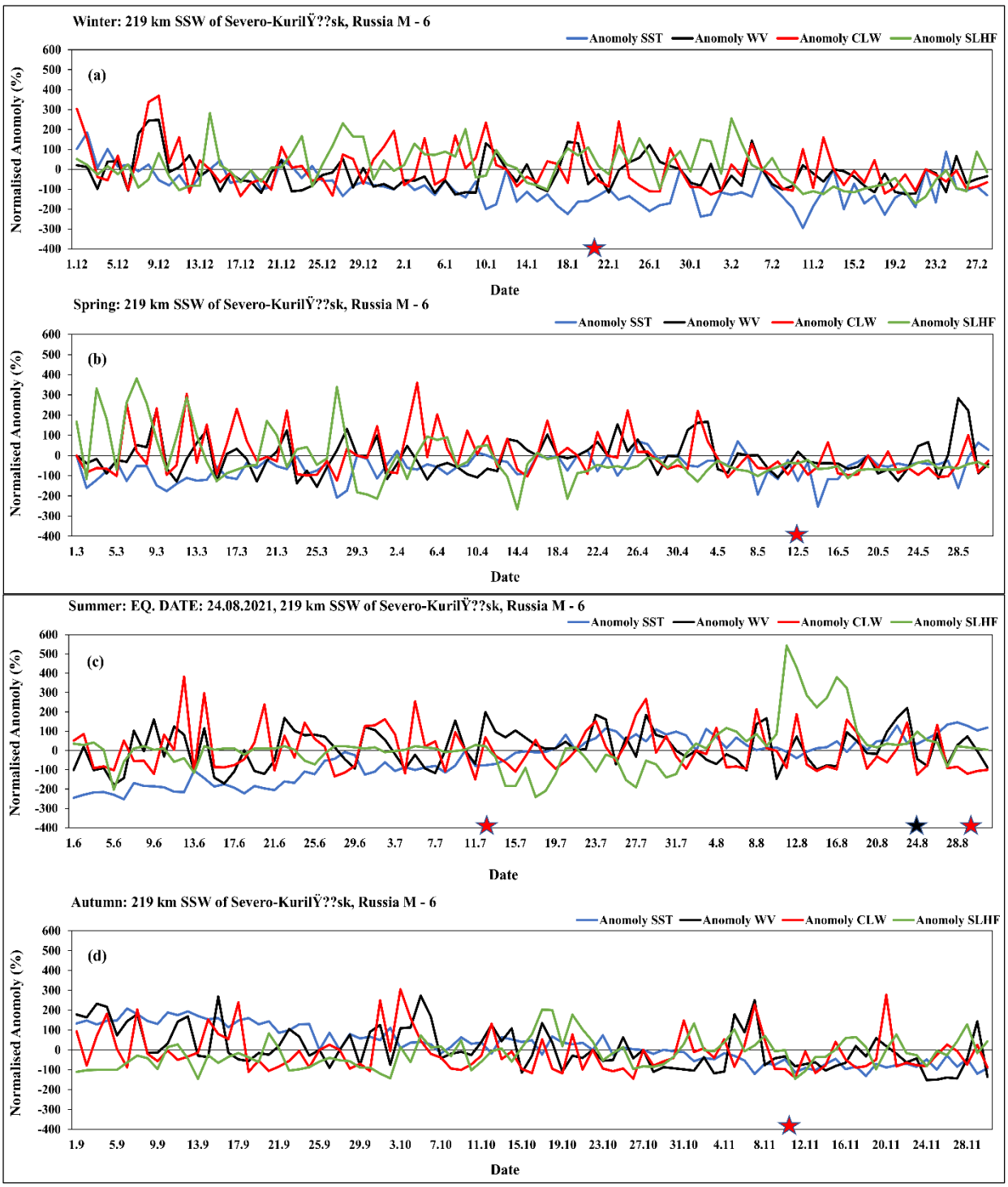

Figure 5. (a), (b), (c), (d) shows the graph of winter, spring, summer and autumn respectively. The black star indicates day of earthquake with M ≥ 6. The red star indicates the day of the earthquake with 4.5 ≤ M < 6. Before the earthquake, SST is followed by SLHF and observed the increments of CLW and Water Vapour.

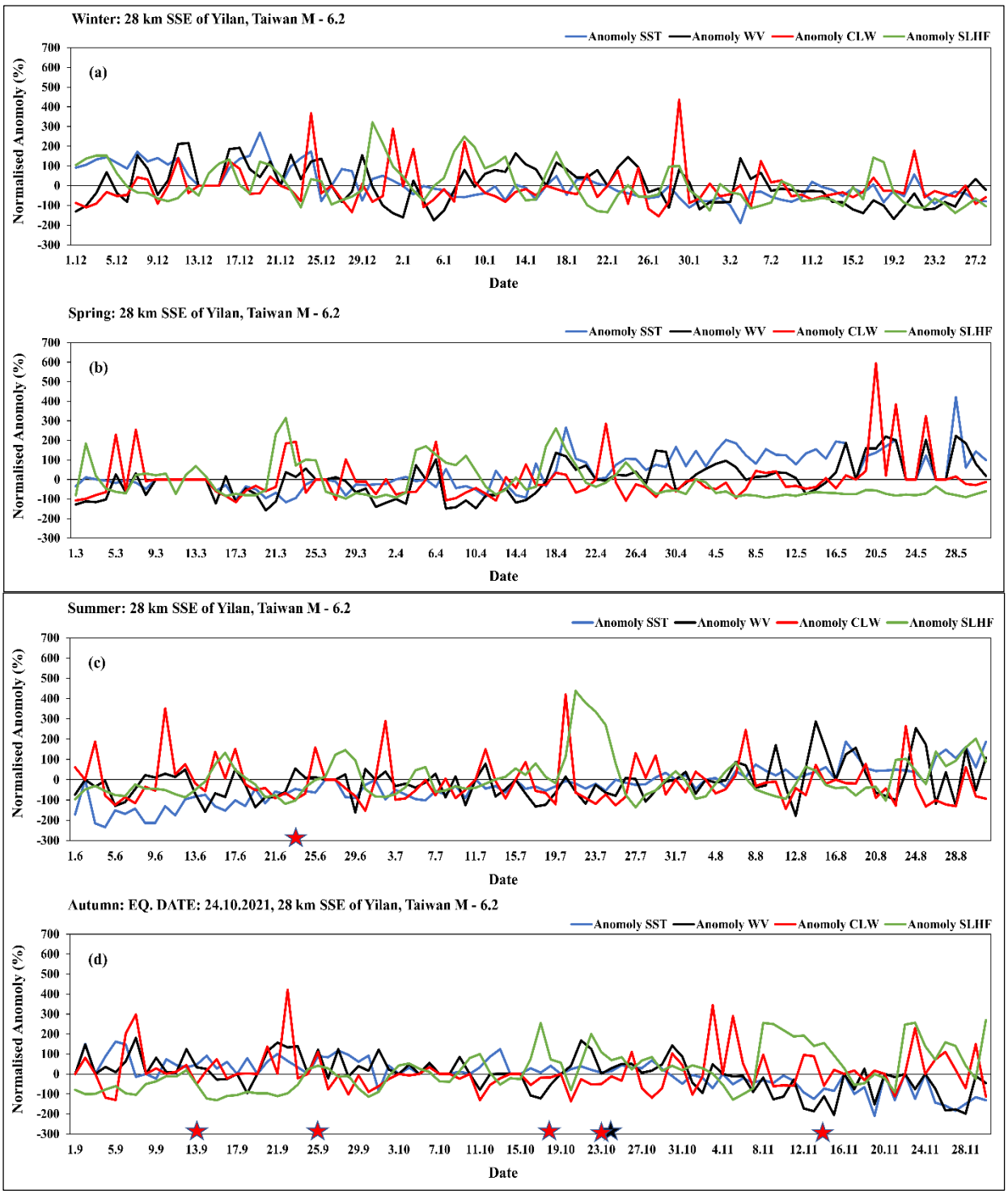

Figure 6. (a), (b), (c), (d) shows the graph of winter, spring, summer and autumn respectively. The black star indicates day of earthquake with M ≥ 6. The red star indicates the day of the earthquake with 4.5 ≤ M < 6. Before the earthquake, SST is followed by SLHF and observed the increments of CLW and Water Vapour.

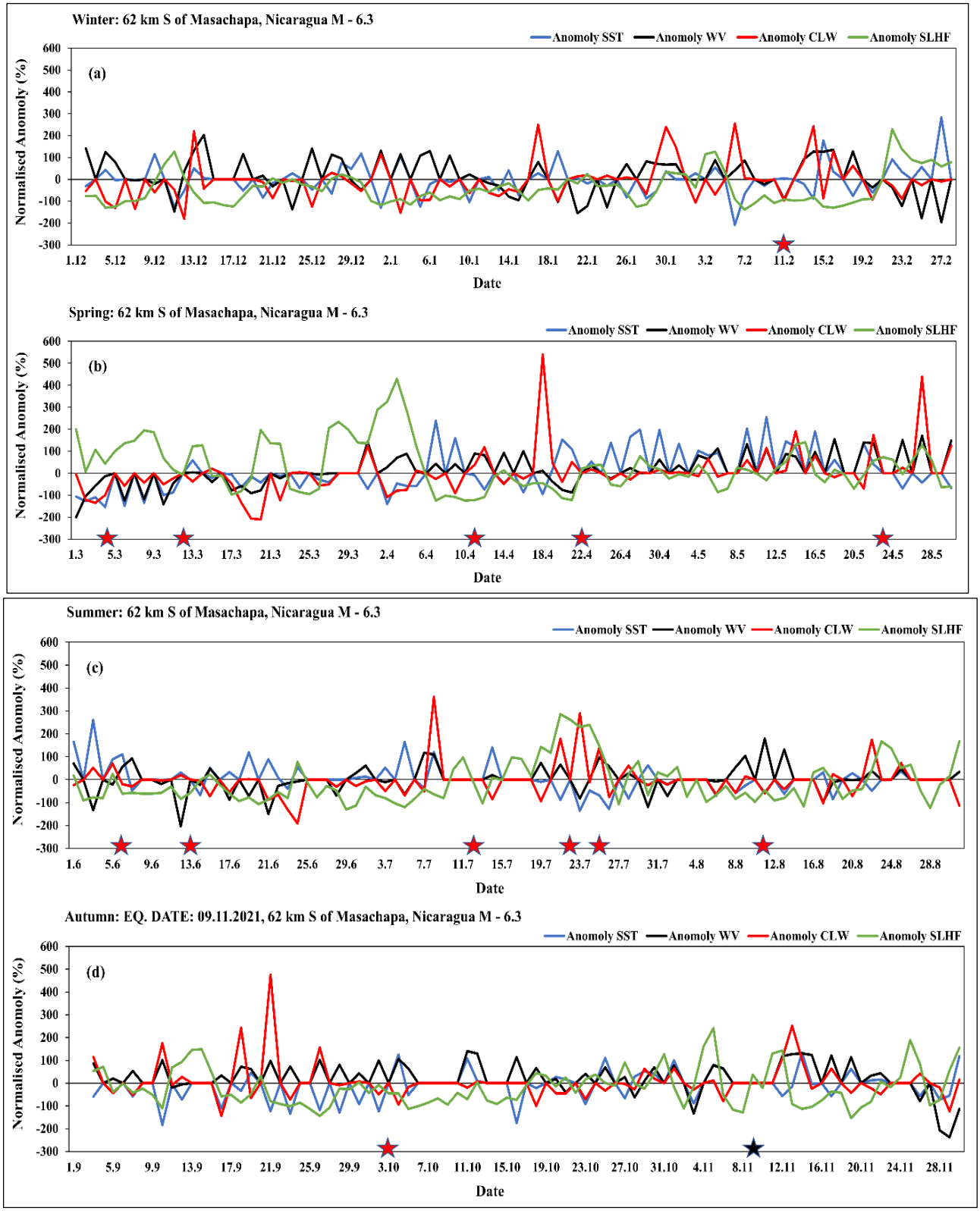

Figure 7. (a), (b), (c), (d) shows the graph of winter, spring, summer and autumn respectively. The black star indicates day of earthquake with M ≥ 6. The red star indicates the day of the earthquake with 4.5 ≤ M < 6. Before the earthquake, SST is followed by SLHF and observed the increments of CLW and Water Vapour.

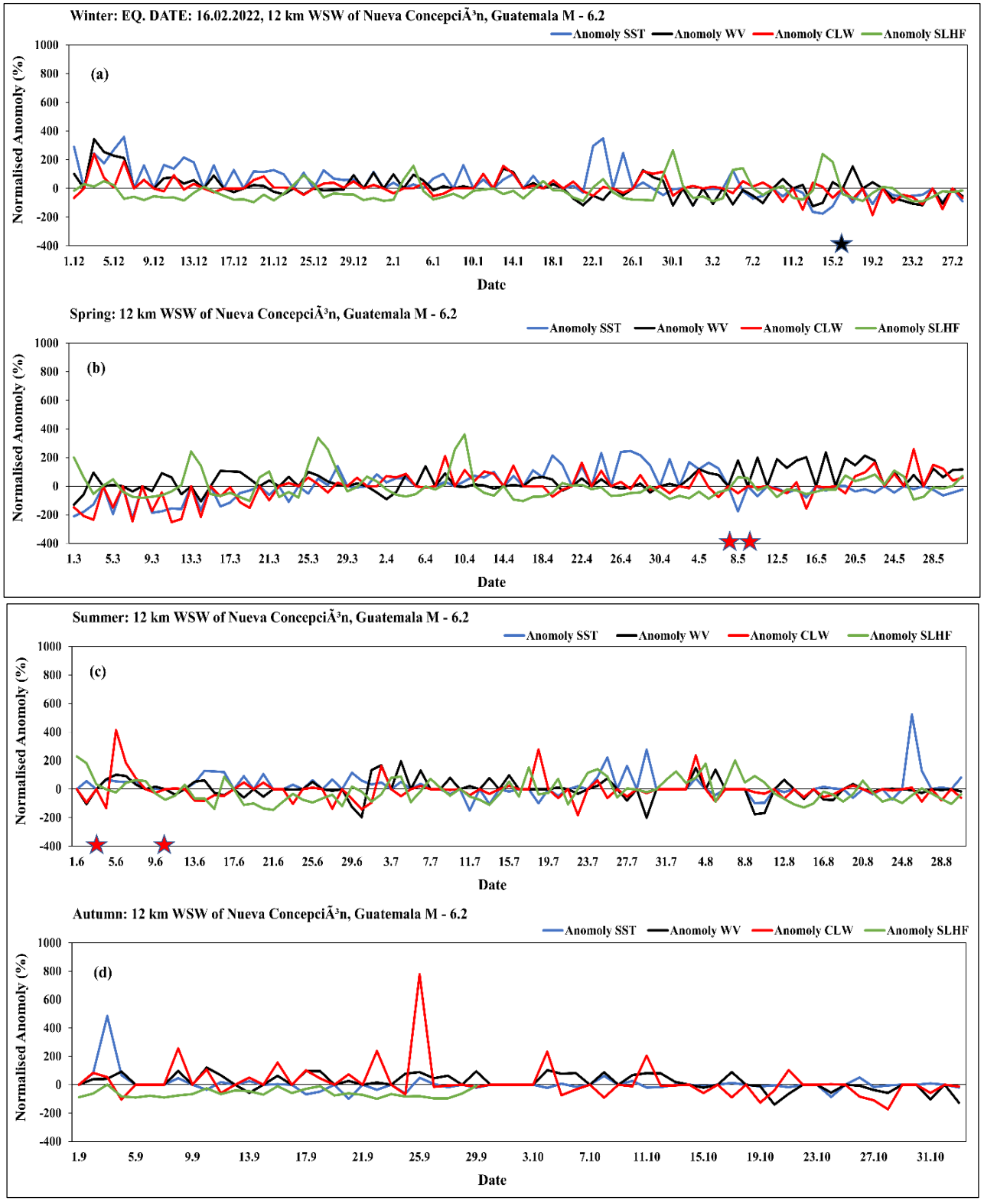

Figure 8. (a), (b), (c), (d) shows the graph of winter, spring, summer and autumn respectively. The black star indicates day of earthquake with M ≥ 6. The red star indicates the day of the earthquake with 4.5 ≤ M < 6. Before the earthquake, SST is followed by SLHF and observed the increments of CLW and Water Vapor.

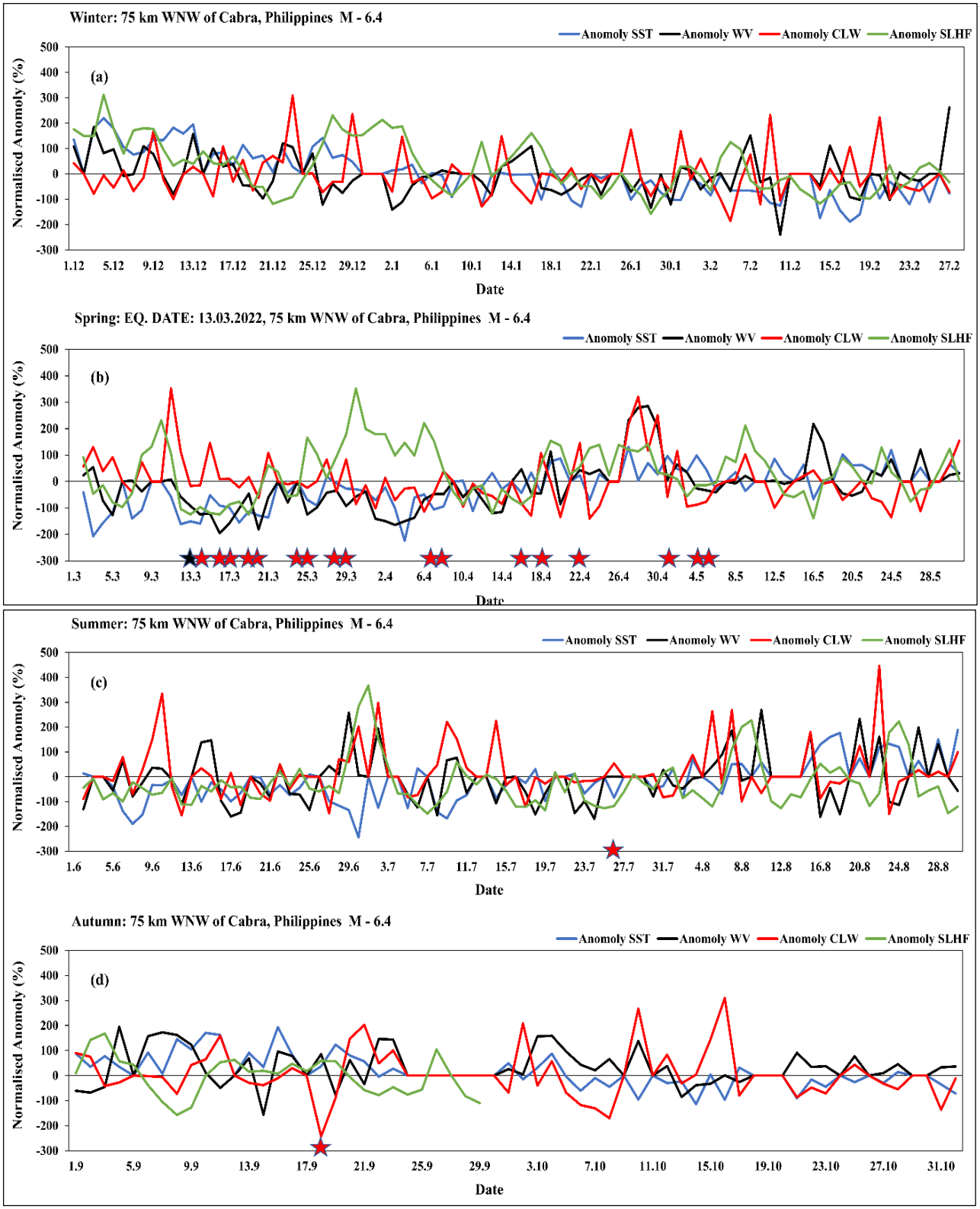

Figure 9. (a), (b), (c), (d) shows the graph of winter, spring, summer and autumn respectively. The black star indicates day of earthquake with M ≥ 6. The red star indicates the day of the earthquake with 4.5 ≤ M < 6. Before the earthquake, SST is followed by SLHF and observed the increments of CLW and Water Vapour.

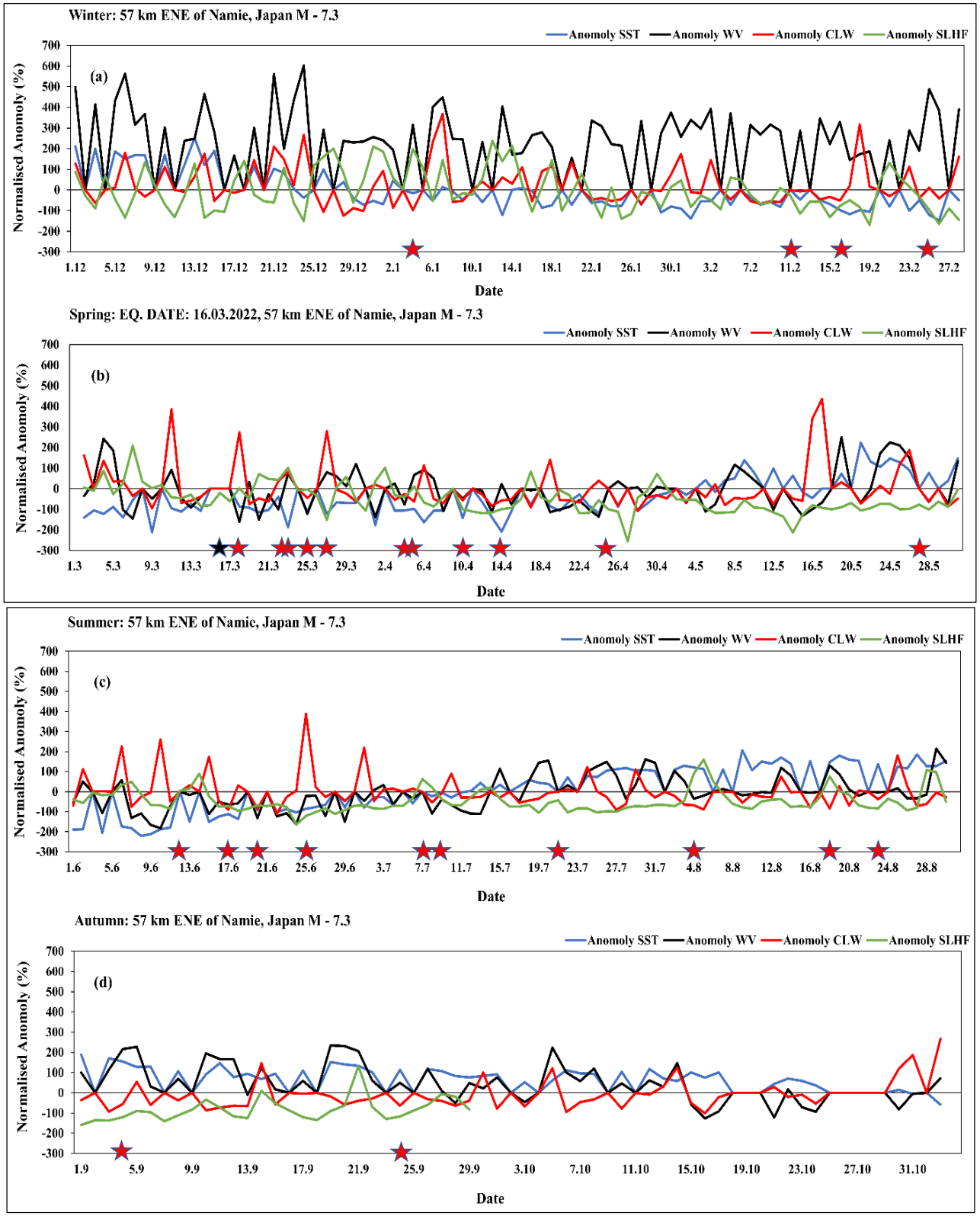

Figure 10. (a), (b), (c), (d) shows the graph of winter, spring, summer and autumn respectively. The black star indicates day of earthquake with M ≥ 6. The red star indicates the day of the earthquake with 4.5 ≤ M < 6. Before the earthquake, SST is followed by SLHF and observed the increments of CLW and Water Vapour.

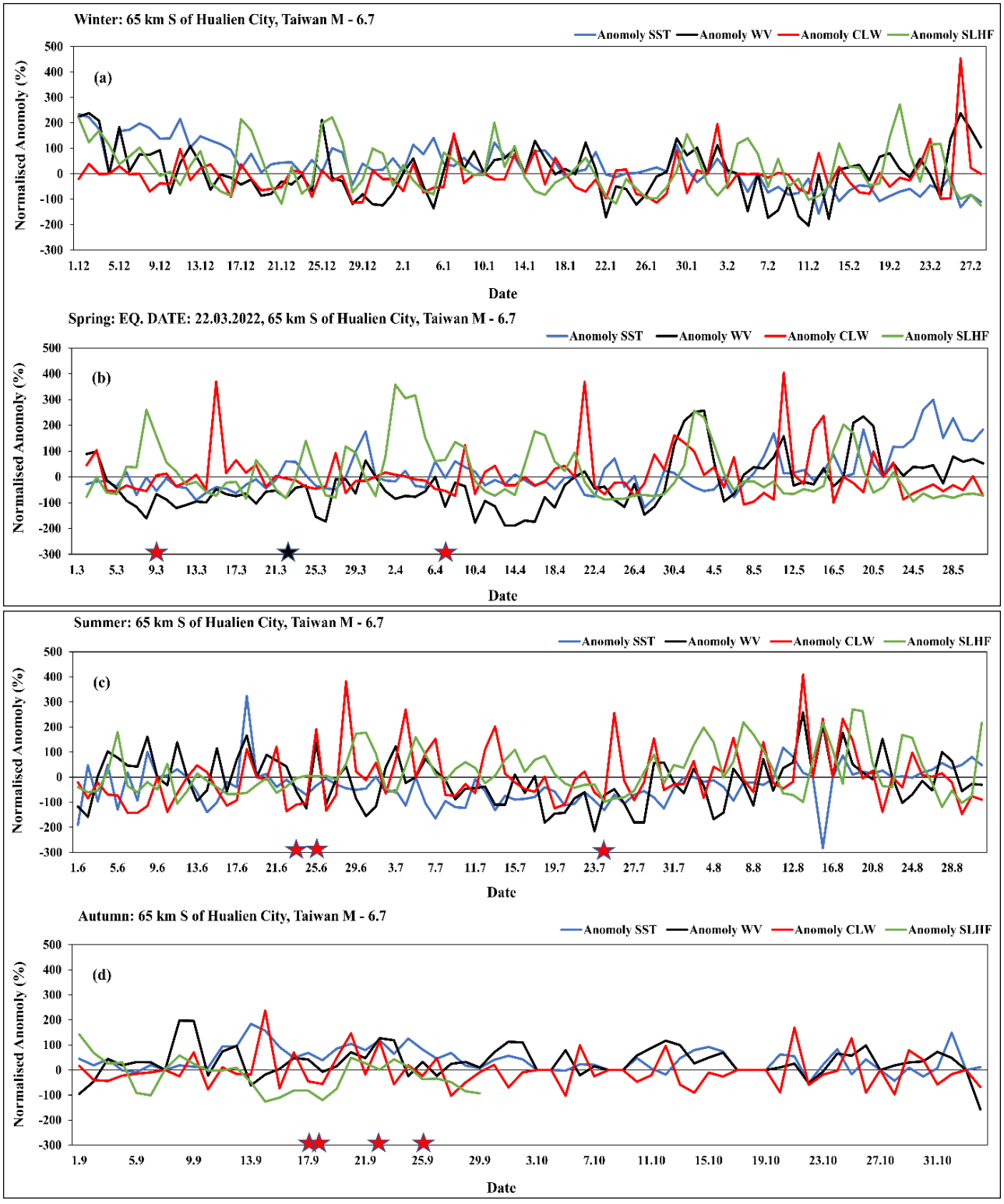

Figure 11. (a), (b), (c), (d) shows the graph of winter, spring, summer and autumn respectively. The black star indicates day of earthquake with M ≥ 6. The red star indicates the day of the earthquake with 4.5 ≤ M < 6. Before the earthquake, SST is followed by SLHF and observed the increments of CLW and Water Vapour.

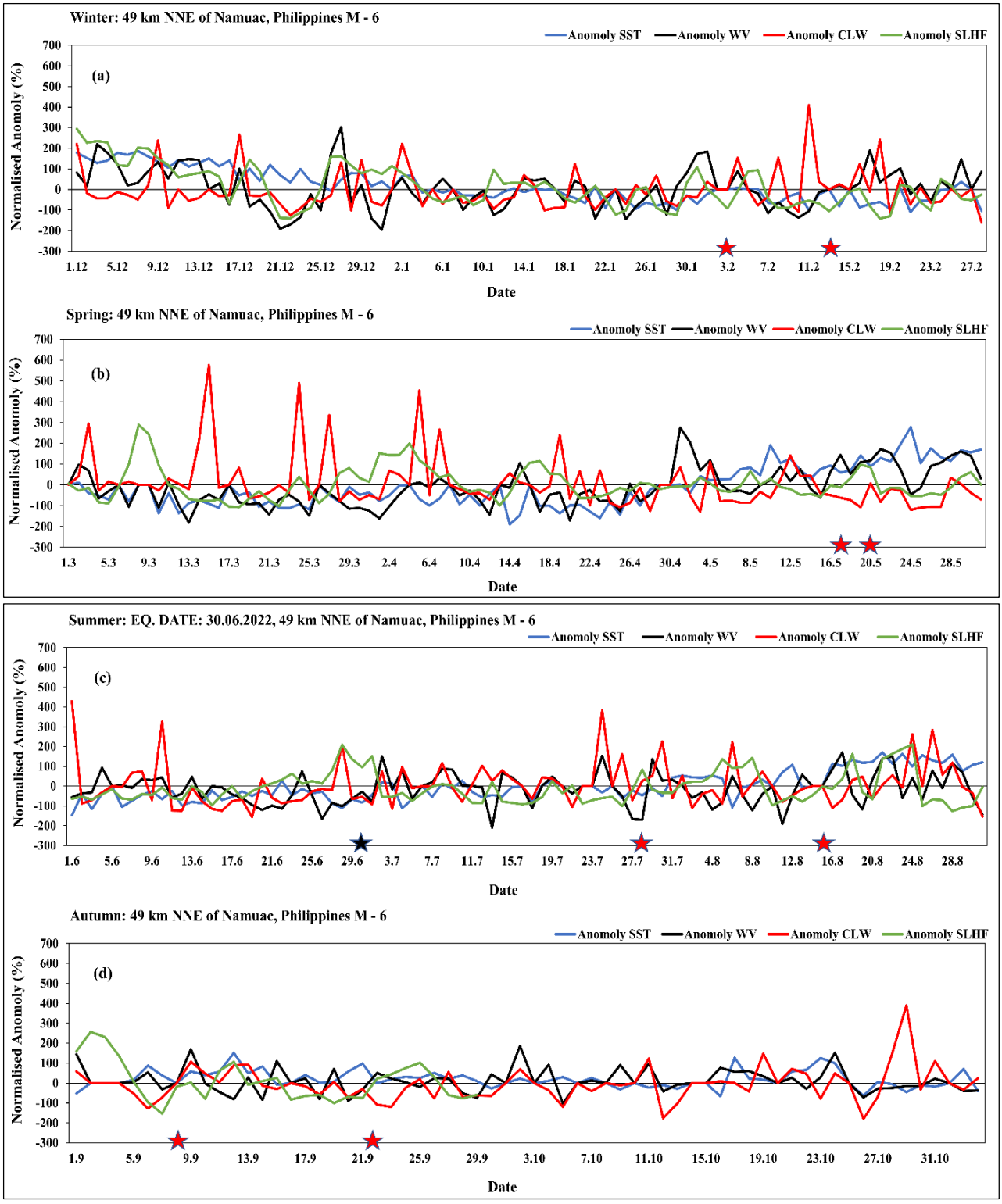

Figure 12. (a), (b), (c), (d) shows the graph of winter, spring, summer and autumn respectively. The black star indicates day of earthquake with M ≥ 6. The red star indicates the day of the earthquake with 4.5 ≤ M < 6. Before the earthquake, SST is followed by SLHF and the increments of CLW and Water Vapour.

Conclusion

This comprehensive study delves into the nuanced variations associated with the eleven coastal earthquakes, specifically examining the intricate relationships among SLHF, SST, CLW, and water vapour. These parameters collectively provide a holistic perspective on the dynamic interplay between land, ocean, and atmospheric conditions. What sets this research apart is the identification of anomalies in SLHF, SST, CLW, and water vapour preceding all eleven earthquakes, presenting a compelling pattern that becomes evident one to eighteen days before the seismic events. A noteworthy observation from this study is the consistent sequence of anomalies leading up to each earthquake. During the initial phase, there is a rise in the temperature of the sea surface, which is followed by a subsequent increase in the surface latent heat flux anomaly. It is important to note that this abnormal

rise in surface latent heat flux is closely connected to the heightened sea surface temperature and the presence of air masses in the coastal region. The anomalies further extend to include an increase in both CLW and water vapour. The observed changes in land, ocean, and atmospheric parameters are interconnected, adding significance to the findings. The anomalies in SLHF, SST, CLW, and water vapour collectively point towards a synchronized response in the coastal environment in the days preceding seismic events. This study, therefore, not only highlights the temporal sequence of anomalies but also emphasizes the interdependency of these factors, providing a more comprehensive understanding of the complex dynamics leading to coastal earthquakes.

Acknowledgment
The Authors acknowledge MCDC for providing the SST, CLW, and Water Vapour data and NOAA for providing the Surface Latent Heat Flux data

References

Bobylev L. P., E. V. Zabolotskikh, I. M. Mitnik and M. L. Mitnik (2009). Atmospheric water vapor and cloud liquid water retrieval over the Arctic Ocean using satellite passive microwave sensing. *IEEE Transactions on Geoscience and Remote Sensing, 48*, 283–294.

Bowen R. (2012). *Surface water*. Springer Science and Business Media.

Chavalier G. (2007). The Earth's Electrical Surface Potential. A Summary of Present Understanding. *California Institute for Human Science, Encinitas, CA*.

Dey S., and R. P. Singh (2003). Surface latent heat flux as an earthquake precursor. *Natural Hazards and Earth System Sciences, 3*, 749–755.

Ghosh S., S. Chowdhury, S. Kundu, S. Sasmal, D. Z. Politis, S. M. Potirakis, . . .S. K. Chakrabarti (2022). Unusual surface latent heat flux variations and their critical dynamics revealed before strong earthquakes. *Entropy, 24*, 23.

Ghosh S., S. Sasmal, S. Chowdhury, S. Chakraborty, T. Basak and S. K. Chakrabarti (2020). Surface Latent Heat Flux Anomaly: A thermal precursory effect of large Earthquake. *2020 URSI Regional Conference on Radio Science (URSI-RCRS)*, (pp. 1–4).

Greenwald T. J., G. L. Stephens, T. H. Vonder Haar and D. L. Jackson (1993). A physical retrieval of cloud liquid water over the global oceans using Special Sensor Microwave/Imager (SSM/I) observations. *Journal of Geophysical Research: Atmospheres, 98*, 18471–18488.

Jie Y. and G. Guangmeng (2014). Brief Communication: An exclusive example of surface latent heat flux variation before Russia M6. 1 earthquake. *Natural Hazards and Earth System Sciences Discussions, 2*, 347–359.

Jing F., X. H. Shen, C. L. Kang and P. Xiong (2013). Variations of multi-parameter observations in atmosphere related to earthquake. *Natural Hazards and Earth System Sciences, 13*, 27–33.

Kumar A. and others. (2021). Long term (1975-2016) anomaly of surface latent heat flux (SLHF) over Indian subcontinent: Signatures of early warning of earthquake disasters. *Indian Journal of Radio & Space Physics (IJRSP), 49*, 19–27.

Liu J. Y., Y. I. Chen, Y. J. Chuo and H. F. Tsai (2001). Variations of ionospheric total electron content during the Chi-Chi earthquake. *Geophysical Research Letters, 28*, 1383–1386.

Ouzounov D. and F. Freund (2001). Ground-atmosphere-ionosphere interactions related to earthquakes: how can earthscope help? *Earthscope Workshop: Making and Breaking a Continent, Report Snowbird, UT, USA.*

Ouzounov, D. and F. Freund (2004). Mid-infrared emission prior to strong earthquakes analyzed by remote sensing data. *Advances in space research, 33*, 268–273.

Ouzounov D., N. Bryant, T. Logan, S. Pulinets and P. Taylor (2006). Satellite thermal IR phenomena associated with some of the major earthquakes in 1999–2003. *Physics and Chemistry of the Earth, Parts A/B/C, 31*, 154–163.

Pulinets S. A. and K. A. Boyarchuk (2004). Ionospheric Precursors of Earthquakes, Springer.

Pulinets S., D. Ouzounov, A. Karelin and D. Davidenko (2018). Lithosphere–atmosphere–ionosphere–magnetosphere coupling—a concept for pre-earthquake signals generation. *Pre-Earthquake Processes: A Multidisciplinary Approach to Earthquake Prediction Studies*, 77–98.

Schulz J., J. Meywerk, S. Ewald and P. Schlüssel (1997). Evaluation of satellite-derived latent heat fluxes. *Journal of Climate, 10*, 2782–2795.

Singh R. P., S. Bhoi, S. and A. K. Sahoo (2001). Significant changes in ocean parameters after the Gujarat earthquake. *Current Science, 80*, 1376–1377.

Singh R. P., S. Bhoi and A.K. Sahoo (2002). Changes observed in land and ocean after Gujarat earthquake of 26 January 2001 using IRS data. *International Journal of Remote Sensing, 23*, 3123–3128.

Singh R. P., G. Cervone, M. Kafatos, A. K. Prasad, A. K .Sahoo, D. Sun, …… and R.yang, R. (2007). Multi-sensor studies of the Sumatra earthquake and tsunami of 26 December 2004. *International Journal of Remote Sensing, 28*, 2885–2896.

Singh R. P., W. Mehdi and M. Sharma (2010). Complementary nature of surface and atmospheric parameters associated with Haiti earthquake of 12 January 2010. *Natural Hazards and Earth System Sciences, 10*, 1299–1305.

Tronin A. A. (1999). Satellite thermal survey application for earthquake prediction. *Atmospheric and ionospheric electromagnetic phenomena associated with earthquakes*.

Tronin A. A. (2000). Thermal IR satellite sensor data application for earthquake research in China. *International Journal of Remote Sensing, 21*, 3169–3177.

Tronin A. A., M. Hayakawa and O.A. Molchanov. (2002). Thermal IR satellite data application for earthquake

research in Japan and China. *Journal of Geodynamics*, *33*, 519–534.

Xu T., Z. Chen, C. Li, J. Wu, Y. Hu and Z. Wu (2011). GPS total electron content and surface latent heat flux variations before the 11 March 2011 M9. 0 Sendai earthquake. *Advances in Space Research*, *48*, 1311–1317.

Xu X., S. Chen, Y. Yu and S. Zhang (2021). Atmospheric Anomaly Analysis Related to Ms> 6.0 Earthquakes in China during 2020–2021. *Remote Sensing*, *13*, 4052.

Yadav K., S. P. Karia and K. N.Pathak (2016). Anomalous Variation in GPS TEC, Land and Ocean Parameters Prior to 3 Earthquakes. *Acta Geophysica*, *64*, 43–60.

Zhang L., M. Jiang and F. Jing (2022). Sea temperature variation associated with the 2021 Haiti M w 7.2 earthquake and possible mechanism. *Geomatics, Natural Hazards and Risk*, *13*, 2840–2863.